Hydrothermal Aluminum-Phosphate-Sulfates in Ash from the 2014 Hydrothermal Eruption at Ontake Volcano, Central Honshu, Japan

minerals

MDPI

Letter

Hydrothermal Aluminum-Phosphate-Sulfates in Ash from the 2014 Hydrothermal Eruption at Ontake Volcano, Central Honshu, Japan

Takumi Imura [1,*], Yusuke Minami [2], Tsukasa Ohba [1], Akiko Matsumoto [3], Antonio Arribas [1] and Mitsuhiro Nakagawa [3]

1 Graduate school of International Resource Sciences, Akita University, Akita 010-8502, Japan
2 Geological Survey of Japan and National Institute of Advanced Industrial Science and Technology (AIST), Ibaraki 305-8567, Japan
3 Graduate School of Science, Hokkaido University, Sapporo 060-0810, Japan
* Correspondence: d6517101@s.akita-u.ac.jp; Tel.: +81-18-889-3193

Received: 9 July 2019; Accepted: 25 July 2019; Published: 29 July 2019

Abstract: Aluminum-phosphate-sulfates (APS) of the alunite supergroup occur in igneous rocks within zones of advanced argillic and silicic alteration in porphyry and epithermal ore environments. In this study we report on the presence of woodhouseite-rich APS in ash from the 27 September 2014 hydrothermal eruption of Ontake volcano. Scanning electron microscope coupled with energy dispersive X-ray spectrometer (SEM-EDS) and field emission (FE)-SEM-EDS observations show two types of occurrence of woodhouseite: (a) as cores within chemically zoned alunite-APS crystals (*Zoned-alunite-woodhouseite-APS*), and (b) as a coherent single-phase mineral in micro-veinlets intergrown with similar micro-veinlets of silica minerals (*Micro-wormy-vein woodhouseite-APS*). The genetic environment of APS minerals at Ontake volcano is that of a highly acidic hydrothermal system existing beneath the volcano summit, formed by condensation in magmatic steam and/or ground waters of sulfur-rich magmatic volatiles exsolved from the magma chamber beneath Mt. Ontake. Under these conditions, an advanced argillic alteration assemblage forms, which is composed of silica, pyrophyllite, alunite and kaolinite/dickite, plus APS, among other minerals. The discovery of woodhouseite in the volcanic ash of the Ontake 2014 hydrothermal eruption represents the first reported presence of APS within an active volcano. Other volcanoes in Japan and elsewhere with similar phreatic eruptions ejecting altered ash fragments will likely contain APS minerals derived from magmatic-hydrothermal systems within the subvolcanic environment. The presence of APS minerals within the advanced argillic zone below the summit vent of Ontake volcano, together with the prior documentation of phyllic and potassically altered ash fragments, provides evidence for the existence within an active volcano in Japan of an alteration column comparable to that of porphyry copper systems globally.

Keywords: aluminum-phosphate-sulfates; alunite; subvolcanic hydrothermal system; Ontake volcano; hydrothermal eruption; phreatic eruption

1. Introduction

Aluminum-phosphate-sulfates minerals (APS) are isostructural with the alunite-jarosite family, within the alunite supergroup. Their chemical formula is generally expressed as $AB_3(XO_4)_2(OH)_6$, where A is a large cation (Na, K, Ag, H_3O, NH_4, Pb, Ca, Ba, Sr, REE) in 12-fold coordination, B is occupied by cations of the elements Al, Fe, Cu, or Zn in octahedral coordination, and X is dominated by S, P, or As [1–5]. This supergroup includes the alunite group (sulfate), beudantite group (phosphate-sulfate), plumbogummite group (phosphate) and dussertite group (arsenate) [2,3,6,7].

Natural APS minerals form complex solid solutions (s.s.) consisting of various endmembers within these groups [8] (Table 1). Chemical varieties of their s.s. compositions reflect varying Eh, fO_2, pH, and activity physicochemical conditions of crystallization within metamorphic, igneous (both plutonic and volcanic), and sedimentary settings [8–14].

APS minerals hosted in igneous rocks typically occur as a result of secondary alteration, whether associated with hydrothermal alteration or with supergene (weathering) in epithermal and porphyry ore systems. Occurrences of APS have been reported in numerous previous studies of ore deposits applying a variety of analytical methods including host-rock petrography, fluid-inclusion geothermometry, and stable isotopic analysis. According to these studies, APS are present in hydrothermally altered volcanic rocks that are altered to advanced argillic and silicic alteration assemblages [15–23]. In these cases, euhedral, commonly bladed, hydrothermal alunite often shows a core of APS with crandallite-woodhouseite-svanbergite (Table 1) compositions [15–23]. APS is detected also along the contact between alkaline-igneous rocks and arigillitic country-rocks, coexisting with cement phased minerals (Calcium Silicate Hydrate (CSH), Calcium Alumium Silicate Hydrate (CASH) [24,25]). Fluid inclusion microthermometry and stable isotopic geothermometry indicate formation temperatures between 200 °C and 350 °C [16,17,23]. Hydrogen, oxygen, and sulfur isotopic studies from APS, and in associated sulfates and sulfides, show that the precipitation of APS is related to mixtures of S-rich magmatic volatiles, hydrothermal fluids, and meteoric groundwaters [15–17,22,23].

Given the similarity in geologic setting, APS minerals should also occur in altered rocks associated with active volcanoes. Samples from some active volcanoes are indeed rich in hydrothermal alunite [26–29]. These products have been interpreted to be derived from sulfuric acid-rich subvolcanic hydrothermal systems. APS from within an active volcano will help understand subvolcanic hydrothermal processes, providing a mineralogical record of the pre-eruptive physicochemical conditions within the subvolcanic hydrothermal system. However, reported occurrences of APS in active volcanic systems have not been reported. This study aims to document the presence of APS mineral in volcanic products from active volcanoes by examining samples of alunite-bearing altered rock from the 2014 hydrothermal eruption of Ontake volcano in central Japan [29].

2. Background of Ontake Volcano, Japan

2.1. Geological Setting

Ontake volcano (3067 MASL), located in central Japan (Figure 1 [30,31]), is a stratovolcano consisting of basalt, andesite, and dacite lava and pyroclastic rocks. This volcano overlies basement rocks composed of Jurassic to Paleogene rhyolitic to rhyodacitic volcanic and marine sedimentary rocks [32,33]. Older volcanic activity at Ontake (200–300 ka) formed an early edifice by effusion of basaltic and andesitic lava with minor dacite [32]. The younger activity (<80 ka) that formed the current edifice is subdivided into an early (78–39 ka) explosive stage of rhyolitic to dacitic magma and a younger (< ~10 ka) stage of effusive andesite lava [33–36]. The summit area around Kengamine peak (Figure 1) is composed of the young andesite lava [32].

During the Holocene, phreatic (or hydrothermal) eruptions have occurred more frequently at Ontake volcano than magmatic eruptions. The frequency of the phreatic (or hydrothermal) eruptions has been estimated to be ~0.6/Ky, double that of the magmatic eruptions [37,38]. Before the 2014 eruption, three phreatic (or hydrothermal) eruptions were witnessed in 1979, 1991, and 2007 [37,39,40], suggesting a higher frequency than 0.6/Ky. Geothermal manifestations have developed on the southwestern flank of Kengamine cone for at least the last 250 years [41]. Hydrothermally altered rocks were exposed in the same area prior to the 2014 eruption.

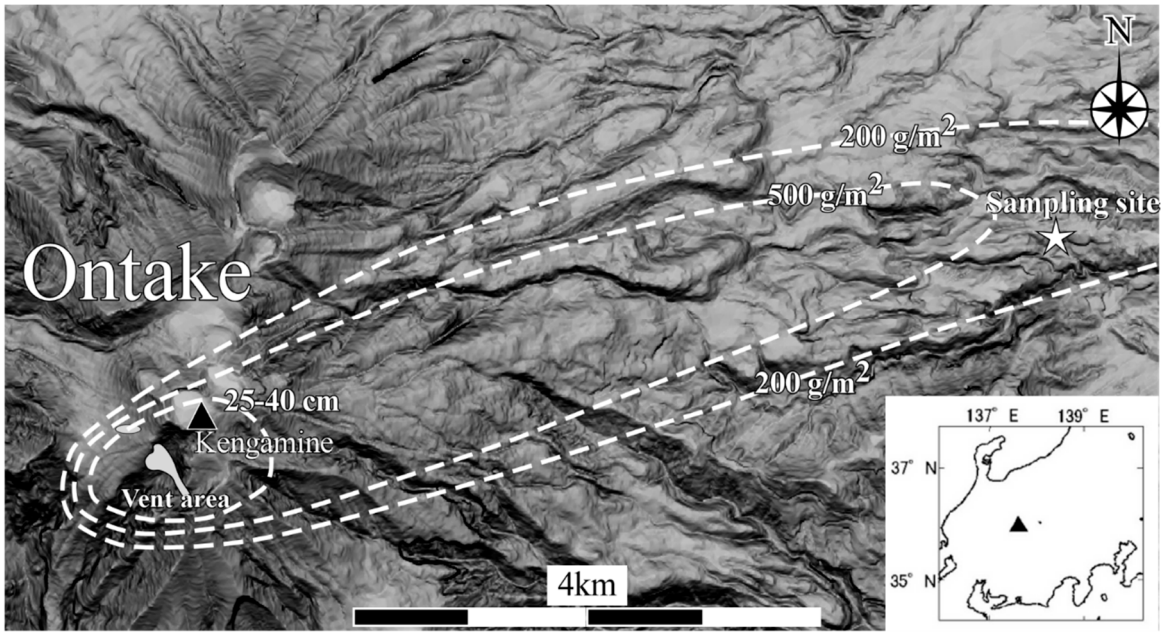

Figure 1. Sampling location of volcanic ash from the 2014 eruption. The topographical relief map is created with Kashimir3D [30] from the 10-m-mesh DEM data provided by the Geospatial Information Authority of Japan. Thickness and isomass contours of the volcanic ash from the 2014 eruption were referred from the results of the geological survey conducted by Earthquake Research Institute, The University of Tokyo (ERI) (2014) [31].

2.2. *Volcanic Ash from the 2014 Hydrothermal Eruption*

The eruption on 27 September 2014 took place on the southwestern flank of Kengamine peak. This eruption ejected approximately one million tonnes of volcanic ash; an estimated volume similar to that of the 1979 eruption [42]. The Volcanic Explosivity Index (VEI) of the 2014 eruption was two [31,43]. The volcanic ash draped the surface of the summit area and the eastern flank [43–45]. Geophysical studies reported precursory seismicity linked to the eruption [46–48].

The ash of the 2014 eruption is composed of abundant altered lithic fragments and minor unaltered volcanic rock fragments [49]. Based on the study of individual ash particles, Minami et al. (2016) [29] classified the alteration into five types: silica–pyrite, silica–pyrite ± alunite ± kaolin, silica–pyrophyllite–pyrite, silica–muscovite ± chlorite, and silica–K-feldspar ± albite ± garnet ± biotite. These results indicate that the ash grains were derived from an active subvolcanic magmatic-hydrothermal system existing under the crater and consisting of silicic, advanced argillic, phyllic, and potassic alteration zones. Minami et al. (2016) [29] interpreted these zones as comparable to the alteration zones in a porphyry copper system [50]. Another study on the volcanic products reported a sulfur isotopic equilibrium temperature of ca. 286 °C, based on the assumption of equilibrium between sulfate (gypsum and anhydrite) and pyrite [51]. These results clearly show that the 2014 eruption was similar to hydrothermal eruption [52] driven by a convecting hot water or steam-dominated hydrothermal system. In this paper we use "hydrothermal eruption [52]" to best describe the 2014 Ontake eruption.

3. Methodology

For this study we used an ash sample documented in Minami et al., (2016) [29]. The sample was collected four days after the eruption, at a roadside point (35°54′29.00″ N, 137°34′06.23″ E) 8 km northeast from the vent (Figure 1). The sample consists mainly of fine (<250 μm) ash. A relatively coarse fraction (70–125 μm) obtained by sieving was prepared for a polished section using epoxy resin. The polished section was observed with a JEOL JSM-6610LV scanning electron microscope (SEM) coupled with an Oxford Instruments energy dispersive X-ray spectrometer (EDS) at Akita University

and a JEOL JSM-7100F field emission (FE) SEM and Oxford Instruments EDS at Hokkaido University. Grain morphological, textural, and petrographic observations were made using backscattered electron images (BEI). Qualitative and semi-quantitative chemical analyses were obtained using the EDS spectra. The analytical instrumental conditions were: 15 kV acceleration voltage, probe current of 2.2 nA (SEM-EDS) and 0.5 nA (FE-SEM-EDS), 10 mm working distance, and a 20 s live time.

4. Results

4.1. Mineral Identification

Semi-quantitative chemical analyses by EDS were carried out to identify APS minerals. APS minerals are defined by the stoichiometric formula (Na, K, Ag, H_3O, NH_4, Pb, Ca, Ba, Sr, REE) (Al, Fe, Cu, and Zn)$_3$ ((S, P, As) O_4) $(OH)_6$ [1–5]. Crystals with spectra consisting of O, S, P, Ca, and Al were identified as APS minerals (Figure 2). In this paper, we use the general name of "APS" to express the designate s.s. between endmember compositions listed in Table 1. For example, the APS crystals consisting mainly of P, S, Ca are denoted by "woodhouseite-APS" (woodhouseite composition-rich APS). Alunite crystals with spectra consisting of O, S, Al, Na, K, and Ca were distinguished from APS (Figure 2; Figure 3). In many cases, these alunite crystals consist of Na-Ca-K in various proportion. We simply express the alunite as the designate s.s. of Na, K, and Ca endmembers (Table 1). For example, Na-K rich alunite is expressed as "Na-K-alunite".

Table 1. Endmember compositions of aluminum-phosphate-sulfates (APS) and alunite.

APS Endmembers		Alunite Subgroup Endmembers	
Svanbergite	$SrAl_3(PO_4)(SO_4)(OH)_6$	Alunite	$KAl_3(SO_4)_2(OH)_6$
Woodhouseite	$CaAl_3(PO_4)(SO_4)(OH)_6$	Huangite	$Ca_{0.5}Al_3(SO_4)_2(OH)_6$
Hinsdalite	$PbAl_3(PO_4)(SO_4)(OH)_6$	Natroalunite	$NaAl_3(SO_4)_2(OH)_6$
Goyazite	$SrAl_3(PO_4)(PO_3OH)(OH)_6$		
Crandallite	$CaAl_3(PO_4)(PO_3OH)(OH)_6$		
Gorceixide	$BaAl_3(PO_4)(PO_3OH)(OH)_6$		
Florencite	$CeAl_3(PO_4)_2(OH)_6$		
Alunite	$KAl_3(SO_4)_2(OH)_6$		
Huangite	$Ca_{0.5}Al_3(SO_4)_2(OH)_6$		
Natroalunite	$NaAl_3(SO_4)_2(OH)_6$		

The selected minerals in Table 1 are referred from [4,6,7].

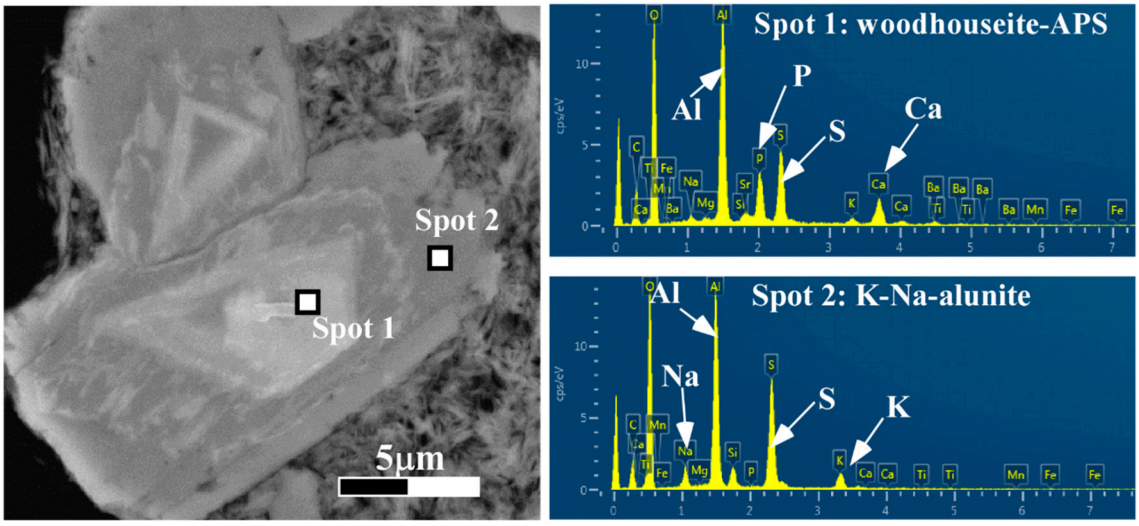

Figure 2. Typical energy dispersive X-ray (EDS) spectrum of aluminum-phosphate-sulfates (APS) mineral occurring as a core of alunite.

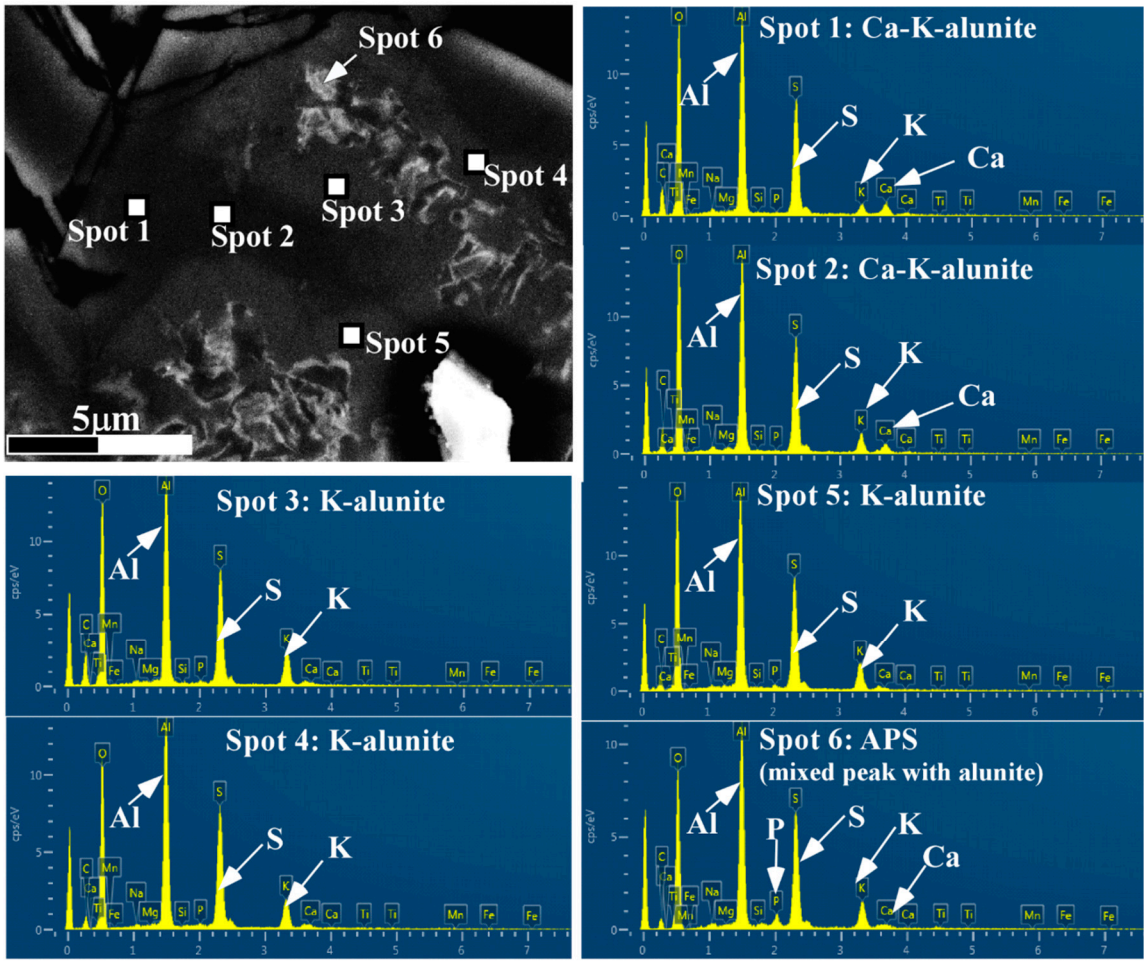

Figure 3. Compositionally zoned alunite containing a core of a dissolved-fibrous APS mineral.

4.2. Petrography of Woodhouseite-APS-Bearing Volcanic Ash Grains

Woodhouseite-APS were observed in the volcanic ash grains altered to advanced argillic and silicic assemblages, as reported by Minami et al. (2016) [29]. The mineral assemblage, alteration type, and occurrence of the woodhouseite-APS in the ash grains studied is summarized in Table 2. Woodhouseite-APS crystals commonly occur as cores of euhedral alunite crystals. Two crystal textures were observed: *Zoned-alunite-woodhouseite-APS* and *Micro-wormy-vein woodhouseite-APS*. The former is more abundant in the examined altered ash grains (Table 2).

Table 2. Summary of petrographical observation on volcanic ash grains.

Ash Grain ID	Minerals in Ash Grains [a]							Alteration [b]	APS Type [c]
	Sil	Kl	Po	Alu	Wod	Py	Ti		
ONTK-VA-001	+			+	+	+	+	RS	ZA
ONTK-VA-002	+			+	+	+		RS	ZA
ONTK-VA-003	+	+						AA	n.d.
ONTK-VA-004				+	+			AA	ZA
ONTK-VA-005	+		+	+	+	+		AA	ZA
ONTK-VA-006	+		+	+				AA-RS	n.d.
ONTK-VA-007	+		+	+				AA-RS	n.d.
ONTK-VA-008	+		+	+				AA-RS	ZA
ONTK-VA-009	+		+	+	+			AA-RS	MW
ONTK-VA-010				+	+			AA	ZA
ONTK-VA-011				+				AA	ZA
ONTK-VA-012	+		+	+	+			AA	ZA
ONTK-VA-013	+		+	+				AA-RS	n.d.

Table 2. *Cont.*

Ash Grain ID	Minerals in Ash Grains [a]							Alteration [b]	APS Type [c]
	Sil	Kl	Po	Alu	Wod	Py	Ti		
ONTK-VA-014	+			+	+		+	RS	n.d.
ONTK-VA-015	+	+			+			AA	MW
ONTK-VA-016				+		+		AA	n.d.
ONTK-VA-017	+		+	+	+	+		AA	ZA

Presence of the minerals in volcanic ash grains are shown by "+" present, and blank. [a] Mineral names are abbreviated as: Sil: silica mineral, Kl: 7-Å kaolin-group mineral, Po: pyrophyllite, Alu: alunite, Wod: woodhouseite-APS, Py: pyrite, and Ti: titanium oxide; [b] RS: residual silicified alteration; AA: advanced argillic alteration; [c] ZA: *Zoned-alunite-woodhouseite-APS*; MW: *Micro-wormy-vein woodhouseite-APS*.

Zoned-alunite-woodhouseite-APS: This type of occurrence is characterized by compositionally zoned alunite crystals. On BEI, the crystal consists of a bright core and a dark rim. As shown in Figure 4 (the EDS elemental intensity profile corresponds to the scan line in the BEI image), the X-ray counts per second (cps) for Ca and P Kα1 peaks are high in the core and low in the rim, whereas those for S, Na, and K show an inverse relationship. This profile indicates that the woodhouseite-APS component (Ca-P and low S) is more abundant in the core than in the rim, which has an alunite composition. Most alunite rims were found to have chemical compositions close to Na-K-alunite.

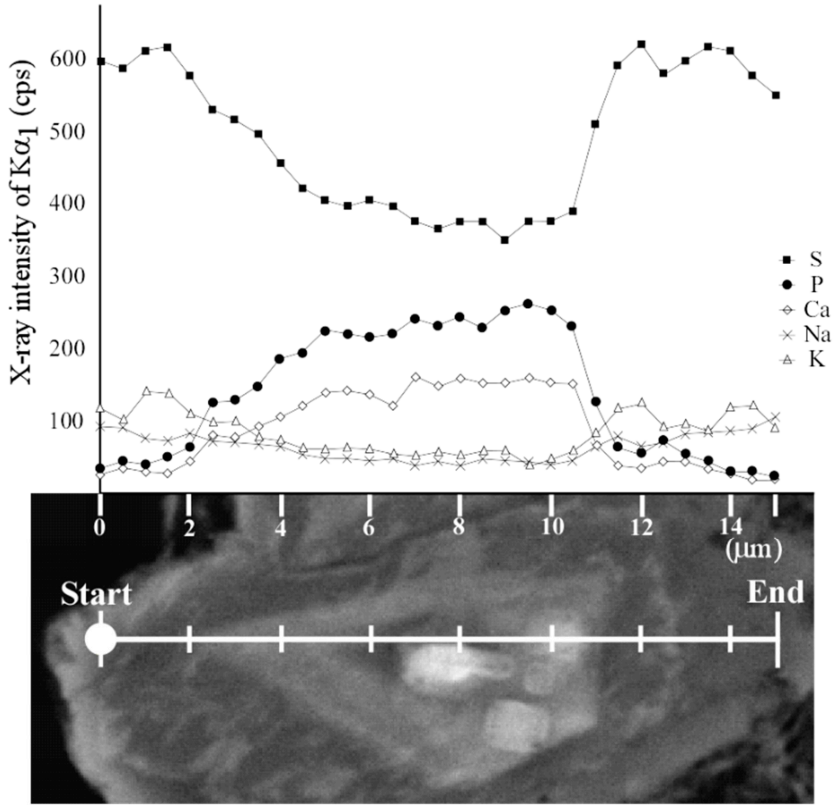

Figure 4. EDS line scan profile with the backscattered electron images (BEI) image of the woodhouseite-bearing alunite crystal. The compositionally zoned crystal is contained in the grain of ONTK-VA-012 in Table 2 and Figure 5b.

Zoned-alunite-woodhouseite-APS appears in a variety of occurrences within ash grains classified as advanced argillically- or residual/vuggy silica-altered, according to Minami et al. (2016) [29]. In one type of occurrence, individual *Zoned-alunite-woodhouseite-APS* crystals typically range between 10 and 50 micrometers in size (Figure 5a,b, Table 2). Within these *Zoned-alunite-woodhouseite-APS* crystals, an internally homogenous core of woodhouseite-APS, which often shows a texture suggesting partial

dissolution, is surrounded by concentric polygons of woodhouseite-APS and, further out, by euhedral alunite (Figure 5b). A fine mixture of silica mineral(s) and pyrophyllite fill the interstitial spaces.

Zoned-alunite-woodhouseite-APS is also observed in irregular aggregates of coarse alunite crystals (Figure 5c,d). In this case, *woodhouseite*-APS occur as what appear to be partially dissolved, often fibrous, clusters within the surrounding alunite, which is typically concentrically zoned. Within the alunite surrounding the *woodhouseite*-APS, the inner rims have a chemical composition closer to K-alunite and the outer rims are closer to Na-Ca-alunite.

Another type of occurrence of *Zoned-alunite-woodhouseite-APS* is shown in Figure 5e,f. The ash grain comprises a massive silicified part and irregular or vein-like open spaces or vugs, which are partially filled with an aggregate of *Zoned-alunite-woodhouseite-APS*. Similar to those described previously, the alunite crystals contain woodhouseite cores. The crystals are smaller (submicron to ca. 10 μm) than the other two types (Figure 5f).

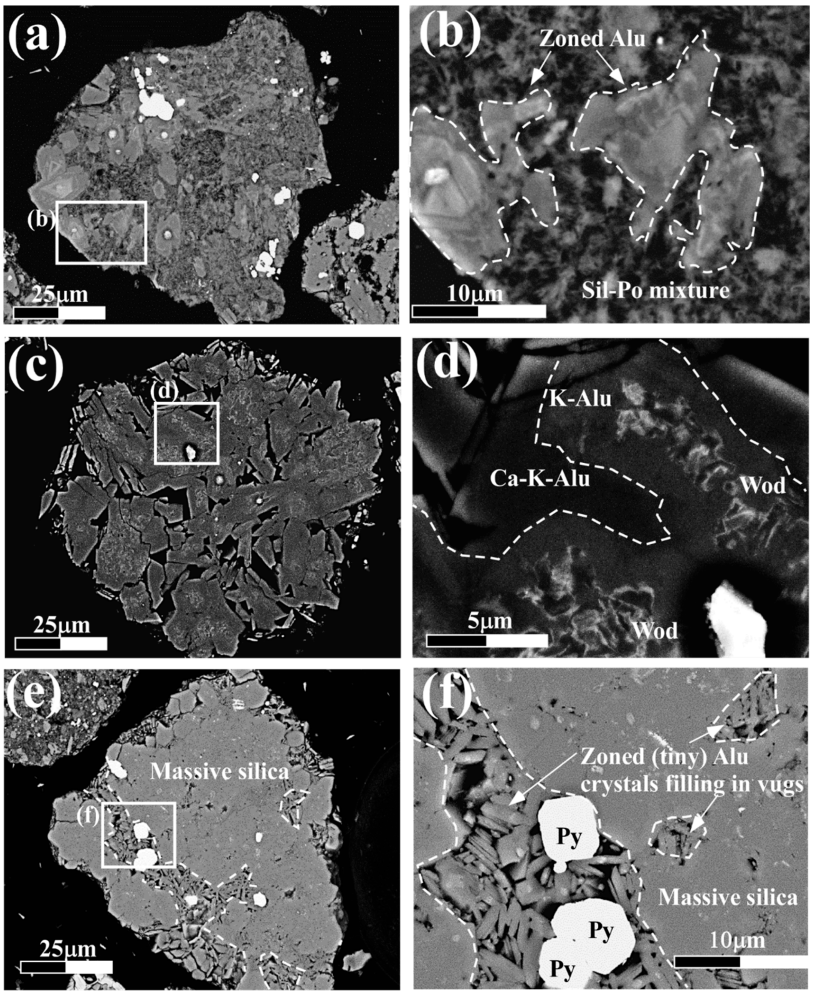

Figure 5. Representative backscattered electron images of *Zoned-alunite-woodhouseite-APS*. Each of (a), (c), and (e) shows the entire view of the ash grain, corresponding respectively to the magnified images of (b), (d), and (f). The mineral abbreviations are the same as in Table 1. (**a**) An aggregate of zoned-alunite crystals in the matrix of silica-pyrophyllite mixture (ONTK-VA-017 in Table 2). (**b**) A fine-grained silica-pyrophyllite mixture interstitially fills among the zoned alunite crystals with a woodhouseite core. (**c**) An aggregate of coarse zoned alunite crystals. (**d**) Zoned alunite containing a fibrous-woodhouseite core (ONTK-VA-004 in Table 2). The interstitial silica and Si-Al clay minerals are not accompanied with the zoned alunite. (**e**) Zoned alunite filling the vugs in a massive silicified rock fragment. Irregular or vein-shaped vugs are incompletely filled with tiny zoned alunite crystals (ONTK-VA-001 in Table 2). (**f**) An aggregate of tiny crystals of zoned alunite in the vugs.

Micro-wormy-vein woodhouseite-APS: In this type of occurrence, the APS mineral forms a coherent single-phase in microveinlets reminiscent of the wormy texture used to describe intergrowths between quartz and advanced argillic alteration minerals, such as pyrophyllite, dickite or alunite, in porphyry copper systems of the Cajamarca region of northern Peru [53]. At Ontake a similar texture is observed in mineral mixtures of silica and woodhousite-APS or kaolinite/dickite (Figure 6a,b). The typical size of the wormy-veins is less than 10 µm in width (Figure 6b). The micro wormy-vein woodhousite-APS texture occurs as an intricate network of silica and woodhouseite-APS with silica occasionally crosscutting the woodhousite-APS.

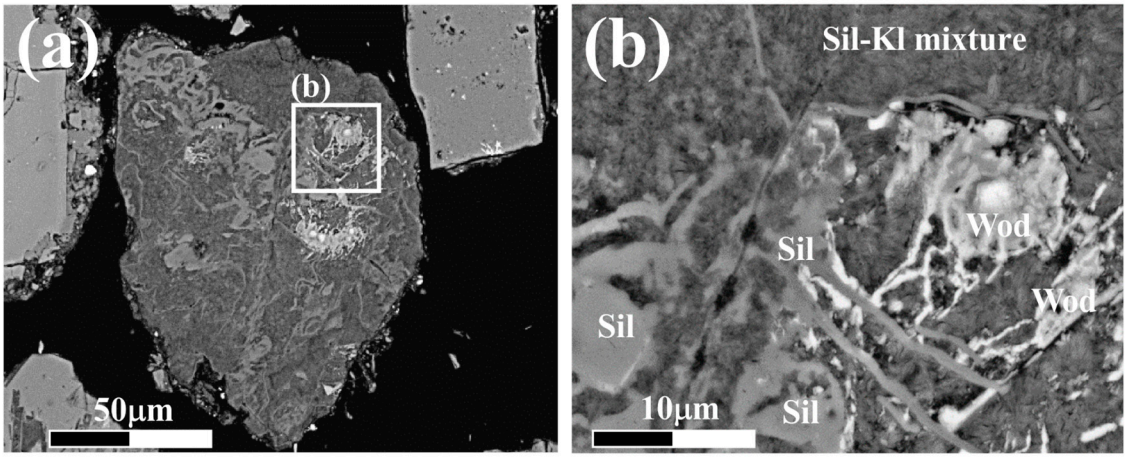

Figure 6. Representative backscattered electron images of *Micro-wormy-vein woodhouseite-APS*. (**a**): entire ash grain containing micro-wormy veins. The grain consists mainly of silica (Sil) and kaolin (Kl) minerals (ONTK-VA-015 in Table 2) (**b**) Micro-wormy vein APS cross-cut by siliceous micro-wormy veins in the matrix of fine-grained silica-kaolin mixtures.

5. Discussion

Phreatic (or hydrothermal) and phreatomagmatic (or magmatic-hydrothermal) eruptions [52] frequently bring to the surface altered lithic fragments from sub-volcanic hydrothermal systems [28,54–56]. The woodhouseite-APS-bearing ash erupted from the September 2014 hydrothermal eruption of Ontake volcano is derived from pre-existing altered rocks under the Kengamine summit crater (Figure 7). They formed in the sub-volcanic environment within an active magmatic-hydrothermal system. The ash grains containing APS minerals consist mainly of hydrothermal minerals including silica, pyrophyllite, kaolinite/dickite, and alunite. The stability temperature conditions of the mineral assemblages in that style of hydrothermal environment ranges between ~150 and 350 °C under highly acidic conditions [57,58]. This temperature range is consistent with the temperature of 286 °C determined by sulfur isotopic fractionation between sulfate and sulfide minerals in volcanic products also from the Ontake 2014 eruption [51]. These genetic conditions indicate a magmatic volatile-rich hydrothermal environment, which is directly comparable with that observed in the early alteration stage of high-sulfidation epithermal ore Au-Cu-Ag-As deposits [59] and the advanced argillic alteration lithocaps above porphyry copper deposits [23,50,60]. They confirm the genetic association proposed among porphyry coppers, some epithermal deposits, and hydrothermal systems within the core of active volcanoes in magmatic arcs [61].

The occurrences described here of both *Zoned-alunite-woodhouseite-APS* and *Micro-wormy-vein woodhouseite-APS* are similar to hydrothermal APS and alunite from epithermal-porphyry ore systems [17,18,22]. For example, both at the Rodalquilar gold-alunite epithermal deposit in Spain [16] and the worldclass Far Southeast (FSE) porphyry Cu-Au-Ag deposit in the Philippines [23], euhedral-bladed hydrothermal alunite contains identical cores of APS minerals (Figure 8). Similarly, hydrothermal APS has also been observed as a monomineralic vein [15] comparable to the *Micro-wormy vein woodhouseite-APS* at Ontake volcano. Although those two types found by this study show different

textures, both types formed under similar genetic conditions within subvolcanic advanced argillic and silicic alteration zones [29].

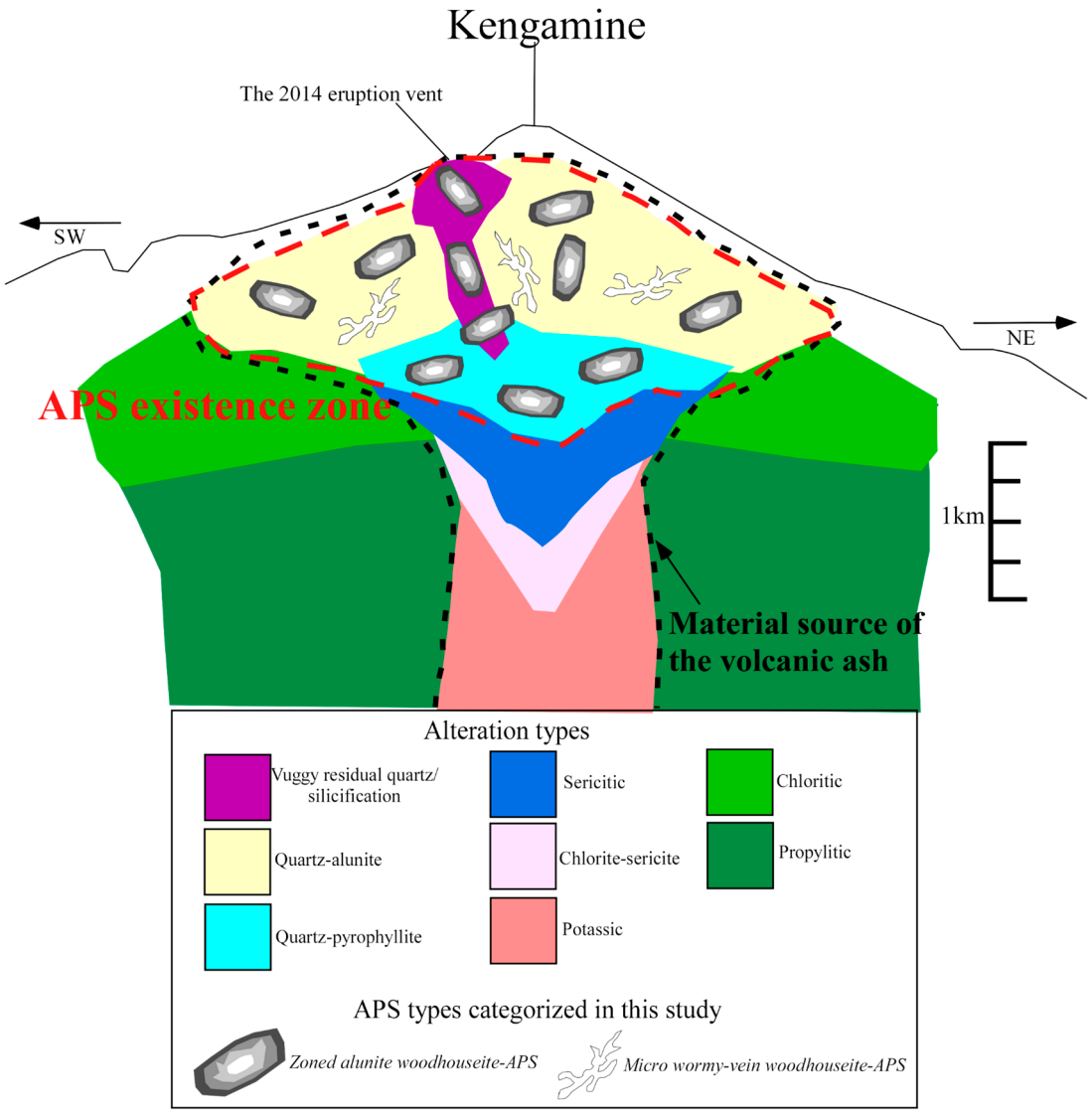

Figure 7. APS existence zone in the material source model (alteration column) of the volcanic ash from the 2014 Ontake eruption. This figure was created and modified from [29,50]. The APS existence zone surrounded by the dashed red line was based on petrography and mineralogy of the individual volcanic ash (Figure 5; Figure 6). The black dotted area is whole material source of the volcanic ash (maximum depth ~2 km) estimated by Minami et al. 2016 [29].

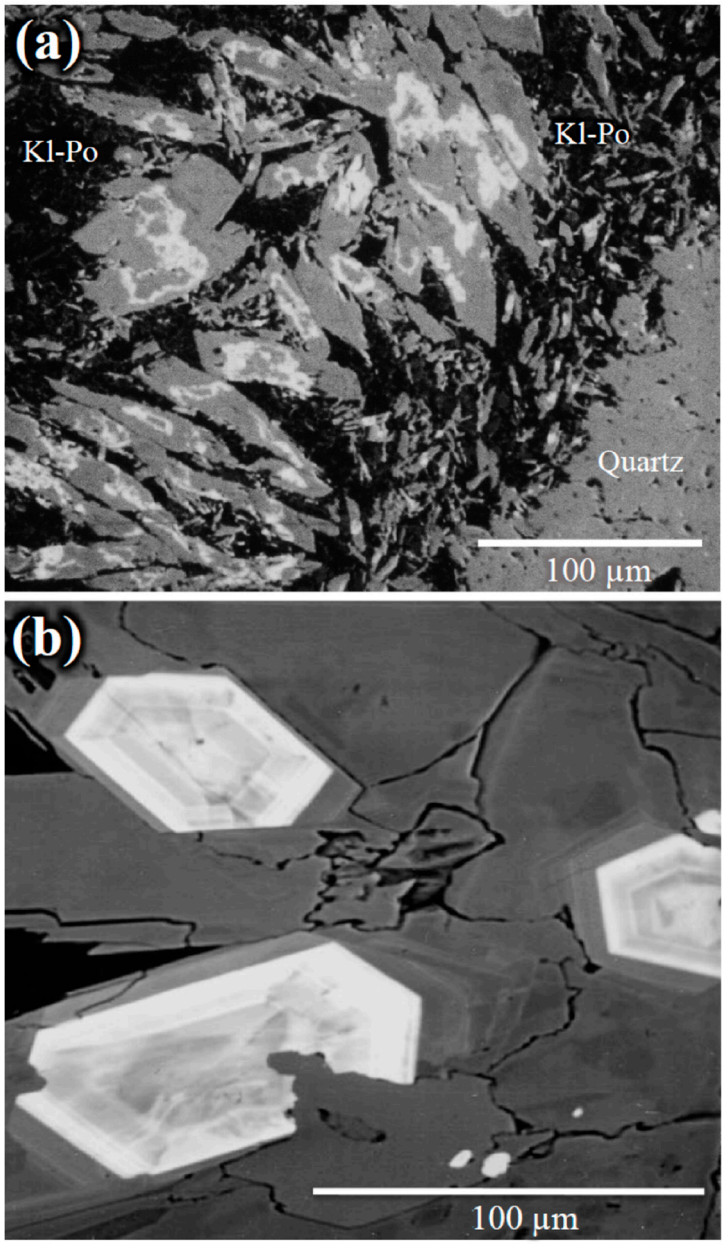

Figure 8. (**a**) Backscattered electron image of bladed-alunite crystals containing dissolved cores of woodhouseite-crandallite-svanbergite accompanying massive quartz within a fine-grained matrix of kaolinite-pyrophyllite (Rodalquilar gold-alunite ore deposit, Spain) [16]. (**b**) Backscattered electron image of alunite and APS minerals from the advanced argillic zone immediately above the FSE porphyry Cu-Au-Ag deposit, Philippines [23]. These photographs are modified and referred from [16] and [23], respectively.

6. Conclusions

The petrographical and mineralogical study of ash grains from the 2014 Ontake volcano hydrothermal eruption resulted in identification of APS minerals such as woodhouseite. Two types of woodhouseite were observed: *Zoned-alunite-woodhouseite-APS* and *Micro-wormy-vein woodhouseite-APS*. The genetic environment of APS minerals is proposed to be highly acidic hydrothermal fluids existing beneath the volcanic summit, formed by condensation with magmatic and/or ground waters of magmatic volatiles exsolved from the magma chamber underneath Ontake volcano. Under these conditions, an advanced argillic alteration assemblage formed consisting of silica, pyrophyllite, alunite, and kaolinite/dickite, plus APS, among other minerals. The 2014 hydrothermal eruption served to

bring to the surface samples of this advanced argillic zone as well as deeper, higher temperature alteration zones [29]. The presence of APS minerals within the advanced argillic zone below the summit vent of Ontake volcano, together with the description of phyllic and potassically altered ash fragments, provides first time evidence for the existence in Japan of an alteration column identical to that of porphyry copper systems globally.

The discovery of woodhouseite in the volcanic ash of the Ontake 2014 hydrothermal eruption represents the first reported presence of APS within an active volcano. As shown in previous studies [26–29] other volcanoes with phreatic (or hydrothermal) eruptions similar to that of Ontake in September 2014 eject altered volcanic products rich in hydrothermal alunite and associated alteration minerals. We believe that further detailed studies will prove that the presence of APS at Ontake is not an exception, but likely commonplace among such active volcanoes.

Author Contributions: T.I. and Y.M. prepared the samples for study, carried out the SEM-EDS and FE-SEM-EDS analyses, and drafted the manuscript. T.O. conceived this study, participated in all steps of the investigation, and helped writing the manuscript. A.M. and M.N. carried out and participated in the FE-SEM-EDS analysis. A.A. provided general research advice and assisted writing the manuscript.

Funding: This research was supported by Ministry of Education, Culture, Sports, Science and Technology-Japan (MEXT) "Integrated Program for Next Generation Volcano Research and Human Resource Development", Japan Society for the Promotion of Science (JSPS) leading program "New Frontier Leader Program for Rare-metals and Resources", "Japan Society for the Promotion of Science Grant-in-Aid for Scientific Research(C) 17K0319", and "Japan Society for the Promotion of Science Grant-in-Aid for Scientific Research(C) 15K01245".

Acknowledgments: We gratefully acknowledge the discussions and significant technical support rendered by Shintaro Hayashi, Takashi Hoshide, Takuya Echigo and Yumi Hayakawa of Akita University.

Conflicts of Interest: The authors declare no conflict of interest.

References

1. Mindat.org. Nickel-Strunz Classification-Primary Groups 10th Edition. 2019. Available online: https://www.mindat.org/strunz.php (accessed on 29 July 2019).
2. Scott, K.M. Solid solution in, and classification of gossan-derived members of the alunite—Jarosite family, Northwest Queensland, Australia. *Am. Mineral.* **1987**, *72*, 178–187.
3. Scott, K.M. The mineralogical distribution of pathfinder elements in gossans derived from dolomitic shale-hosted Pb-Zn deposits, Northwest Queensland, Australia. *Chem. Geol.* **1987**, *64*, 295–306. [CrossRef]
4. Stoffregen, R.E.; Alpers, C.N. Woodhouseite and svanbergite in hydrothermal ore deposits: products of apatite destruction during advanced argillic alteration. *Can. Mineral.* **1987**, *25*, 201–211.
5. Smith, D.K.; Roberts, A.C.; Bayliss, P.; Liebau, F. A systematic approach to general and structure-type formulas for minerals and other inorganic phases. *Am Mineral.* **1998**, *83*, 126–132. [CrossRef]
6. Mills, S.J.; Hatert, F.; Nickel, E.H.; Ferraris, G. The standardisation of mineralgroup hierarchies: Application to recent nomenclature proposals. *Eur. J. Miner.* **2009**, *21*, 1073–1080. [CrossRef]
7. Bayliss, P.; Kolitsch, U.; Pring, A. Alunite supergroup: Recommended nomenclature. *Miner. Mag.* **2010**, *74*, 919–927. [CrossRef]
8. Dill, H.G. The geology of aluminum phosphate and sulphates of the alunite group minerals: A review. *Earth-Sci. Rev.* **2001**, *53*, 35–93. [CrossRef]
9. Heald, P.; Foley, N.K.; Hyaba, D.O. Comparative anatomy of volcanic-hosted epithermal deposits: Acid-sulphate and adularia-sulfate types. *Econ. Geol.* **1987**, *82*, 11–26. [CrossRef]
10. Stoffregen, R.E.; Cygan, G.L. An experimental study of Na-K exchange between alunite and aqueous sulfate solutions. *Am. Mineral.* **1990**, *75*, 209–220.
11. Stoffregen, R.E.; Rye, R.O.; Wasserman, M.D. Experimental studies of aluntie: I ^{18}O-^{16}O and DH fractionation factors between alunite and water at 250–450 °C. *Geochim. Cosmochim. Acta* **1994**, *58*, 903–916. [CrossRef]
12. Beaufort, D.; Patrier, P.; Laverret, E.; Bruneton, P.; Mondy, J. Clay alteration associated with proterozoic unconformity-type uranium deposits in the East Alligator Rivers Uranium Field, Northern Territory, Australia. *Econ. Geol.* **2005**, *100*, 515–536. [CrossRef]

13. Gaboreau, S.; Beaufort, D.; Vieillard, P.; Partrier, P. Aluminum phosphate-sulfate minerals associated with Proterozoic unconformity-type uranium deposits in the East Alligator River Uranium Field, Northern Territories, Australia. *Can. Mineral.* **2005**, *43*, 813–827. [CrossRef]
14. Gaboreau, S.; Cuney, M.; Quirt, D.; Beaufort, D.; Patrier, P.; Mathieu, D. Significance of aluminum phosphate-sulfate minerals associated with U unconformity-type deposits: The Athabasca basin, Canada. *Am. Mineral.* **2007**, *92*, 267–280. [CrossRef]
15. Aoki, M.; Comsti, E.C.; Lazo, F.B. Advanced argillic alteration and geochemistry of alunite in an evolving hydrothermal system at Baguio, Northern Luzon, Philippines. *Resour. Geol.* **1993**, *43*, 155–164.
16. Arribas, A., Jr.; Cunningham, C.G.; Rytuba, J.J.; Rye, R.O.; Kelly, W.C.; Podwysocki, M.H.; McKee, E.H.; Tosdal, R.M. Geology, geochemistry, fluid inclusions and isotope geochemistry of the Rodalquilar gold alunite deposit, Spain. *Econ. Geol.* **1995**, *90*, 795–822. [CrossRef]
17. Hedenquist, J.W.; Matsuhisa, Y.; Izawa, E.; White, N.C.; Giggenbach, W.F.; Aoki, M. Geology, geochemistry, and origin of high sulphidation Cu-Au mineralization in the Nansatsu District, Japan. *Econ. Geol.* **1994**, *89*, 1–30. [CrossRef]
18. Matsubara, S.; Matsuyama, F.; Kiyota, K.; Kato, A. Huangite from okumanza, gunnma prefecture, Japan. *Mineral. Mag.* **1998**, *20*, 123–135.
19. Dill, H.G.; Fricke, A.; Hening, K.-H. The origin of Ba- and REE-bearing aluminium-phosphate-sulphate minerals from the Lohrheim kaolinitic clay deposit (Rheinisches Schiefergebirge, Germany). *Appl. Clay. Sci.* **1995**, *10*, 231–245. [CrossRef]
20. Dill, H.G.; Bosse, H.-R.; Henning, K.-H.; Fricke, A.; Ahrend, H. Mineralogical and chemical variations in hypogene and supergene kaolin deposits in a mobile fold belt—The Central Andes of northwestern Peru. *Miner. Depos.* **1997**, *32*, 149–163. [CrossRef]
21. Dill, H.G.; Bosse, H.-R.; Kassbohm, J. Mineralogical and chemical studies of volcanic-related argillaceous industrial minerals of the Central American Cordillera (western El Salvador). *Econ. Geol.* **2000**, *95*, 517–538. [CrossRef]
22. Ando, Y.; Tsutsumi, S. Acid alteration and geochemistry of alunite in the western Izu Peninsula, Shizuoka Prefecture. *Jpn. Mag. Miner. Petrol. Sci.* **2005**, *34*, 59–68, (In Japanese with English abstract).
23. Hedenquist, J.W.; Arribas, A., Jr.; Aoki, M. Zonation of sulfate and sulfide minerals and isotopic composition inc the Far Southeast Porphyry and Lepanto epithermal Cu-Au deposits, Philippines. *Resour. Geol.* **2017**, *67*, 174–196. [CrossRef]
24. Stoppa, F.; Scordari, F.; Mesto, E.; Sharygin, V.V.; Bortolozzi, G. Calcium-aluminum-silicate-hydrate "cement" phases and rare Ca-zeolite association at Colle Fabbri, Central Italy. *Open Geosci.* **2010**, *2*, 175–187. [CrossRef]
25. Stoppa, F.; Schiazza, M. Extreme chemical conditions of crystallization of Umbrian Melilitolites and wealth of rare, late stage/hydrothermal minerals. *Cent. Eur. J. Geosci.* **2014**, *6*, 549–564. [CrossRef]
26. Takano, B.; Watanuki, K. Monitoring of volcanic eruptions at Yugama crater lake by aqueous sulphur oxyanions. *J. Volcanol. Geotherm. Res.* **1990**, *40*, 71–87. [CrossRef]
27. Tomita, K.; Kawano, M.; Kobayashi, T. Minerals in the volcanic ash erupted from Shin-dake in Kuchinoerabu Island in 1980—Report of the Faculty of Science, Kagoshima University. *Earth Sci. Biol.* **1994**, *27*, 1–10.
28. Ohba, T.; Kitade, Y. Subvolcanic hydrothermal systems: Implications from hydrothermal minerals in hydrovolcanic ash. *J. Volcanol. Geotherm. Res.* **2005**, *145*, 249–262. [CrossRef]
29. Minami, Y.; Imura, T.; Hayashi, S.; Ohba, T. Mineralogical study on volcanic ash of the eruption on September 27, 2014 at Ontake volcano, central Japan: Correlation with porphyry copper systems. *Earth Planets Space* **2016**, *68*, 67. [CrossRef]
30. Sugimoto, T. Kashimir 3D Ver 9.2.8 23819 (9.2.8). Available online: http://www.kashmir3d.com/ (accessed on 3 July 2018).
31. Earthquake Research Institute at the University of Tokyo (ERI): Eruption of the Ontakesan. 27 September 2014. Available online: http://www.eri.u-tokyo.ac.jp/en/2014/09/30/eruption-of-the-ontakesan-27th-september-2014/ (accessed on 6 July 2018).
32. Yamada, N.; Kobayashi, T. *Geology of the Ontakesan District. Geological Sheet Map at 1:50,000*; Geological Survey of Japan: Tsukuba, Japan, 1988; (In Japanese with English abstract).
33. Takeuchi, M.; Nakano, S.; Harayama, S.; Otuska, T. *Geology of the Kiso-Fukushima District. With Geological Sheet Map at 1:50,000*; Geological Survey of Japan: Tsukuba, Japan, 1998; (In Japanese with English abstract).

34. Matsumoto, A.; Kobayashi, T. K-Ar age determination of late Quaternary volcanic rocks using the "mass fractionation correction procedure": Application to the Younger Ontake Volcano, central Japan. *Chem. Geol.* **1995**, *125*, 123–135, (In Japanese with English abstract). [CrossRef]
35. Matsumoto, A.; Kobayashi, T. K-Ar ages of the older Ontake volcanic products, Ontake volcano, central Japan: Reappraisal of the volcanic history based on the radiometric data. *Bull. Volcanol. Soc. Japan* **1999**, *44*, 1–12, (In Japanese with English abstract).
36. Kioka, H.; Furuyama, K.; Miyake, Y.; Sakai, I.; Nagao, K.; Ikemoto, M.; Noiri, H.; Oda, K. K-Ar chronology of the Middle Pleistocene lavas at Ontake Volcano, central Japan. *Earth. Sci. (Chikyu Kagaku)* **1998**, *52*, 464–474.
37. Oikawa, T.; Suzuki, Y.; Chiba, T. Eruptions of Ontake-san: History and 2014 eruption. *Kagaku* **2014**, *84*, 1218–1225. (In Japanese)
38. Oikawa, T.; Yamaoka, K.; Yoshimoto, M.; Nakada, S.; Takeshita, Y.; Maeno, F.; Ishizuka, Y.; Komori, J.; Shimano, T.; Nakano, S. The 2014 eruption of Ontake volcano, Central Japan. *Bull. Volcanol. Soc. Japan* **2015**, *60*, 411–415, (In Japanese with English abstract).
39. Japan Meteorological Agency (JMA). Ontake volcano. *Bull. Volcanol. Soc. Japan* **1991**, *36*, 385. (In Japanese)
40. Nakamichi, H.; Kumagai, H.; Nakano, M.; Okubo, M.; Kimata, F.; Ito, Y.; Obara, K. Source mechanism of very-long-period event at Mt. Ontake, central Japan: Response of a hydrothermal system to magma intrusion beneath the summit. *J. Volcanol. Geotherm. Res.* **2009**, *187*, 167–177. [CrossRef]
41. Oikawa, T. Reinvestigation of the historical eruption and fumarolic activity records at Ontake Volcano, central Japan—Misunderstanding reports about the 774 AD and 1892 AD eruptions. *Bull. Geol. Surv. Japan* **2008**, *59*, 203–210. [CrossRef]
42. Takarada, S.; Oikawa, T.; Furukawa, R.; Hoshizumi, H.; Itoh, J.; Geshi, N.; Miyagi, I. Estimation of total discharged mass from the phreatic eruption of Ontake Volcano, central Japan, on September 27, 2014. *Earth Planets Space* **2016**, *68*, 138. [CrossRef]
43. Japan Meteorological Agency (JMA)—Report of Coordinating Committee for Prediction of Volcanic Eruption. 2014. Available online: http://www.data.jma.go.jp/svd/vois/data/tokyo/STOCK/kaisetsu/CCPVE/shiryo/130/130_no01.pdf (accessed on 6 July 2018). (In Japanese).
44. Maeno, F.; Nakada, S.; Oikawa, T.; Yoshimoto, M.; Komori, J.; Ishizuka, Y.; Takeshita, Y.; Shimano, T.; Kaneko, T.; Nagai, M. Reconstruction of a phreatic eruption on 27 September 2014 at Ontake volcano, central Japan, based on proximal pyroclastic density current and fallout deposits. *Earth Planets Space* **2016**, *68*, 82. [CrossRef]
45. Oikawa, T.; Yoshimoto, M.; Nakada, S.; Maeno, F.; Komori, J.; Shimano, T.; Takeshita, Y.; Ishizuka, Y.; Ishimine, Y. Reconstruction of the 2014 eruption sequence of Ontake Volcano from recorded images and interviews. *Earth Planets Space* **2016**, *68*, 79. [CrossRef]
46. Kato, A.; Terakawa, T.; Yamanaka, Y.; Maeda, Y.; Horikawa, S.; Matsuhiro, K.; Okuda, T. Preparatory and precursory processes leadingup to the 2014 phreatic eruption of Mount Ontake, Japan. *Earth Planets Space* **2015**, *67*, 111. [CrossRef]
47. Maeda, Y.; Kato, A.; Terakawa, T.; Yamanaka, Y.; Horikawa, Y.; Matsuhiro, K.; Okuda, T. Source mechanism of a VLP event immediately before the 2014 eruption of Mt. Ontake, Japan. *Earth Planets Space* **2015**, *67*, 187. [CrossRef]
48. Ogiso, M.; Matsubayashi, H.; Yamamoto, T. Descent of tremor source locations before the 2014 phreatic eruption of Ontake volcano, Japan. *Earth Planets Space* **2015**, *67*, 206. [CrossRef]
49. Miyagi, I.; Geshi, N.; Hamasaki, S.; Tomiya, A. Volcanic ash particles from Ontake volcano on September 2014. In *Emergency academic session in the Volcanological Society of Japan 2014 fall meeting, Supplement: Emergency Academic Session*; Fukuoka University: Fukuoka, Japan, 2014; pp. 2–4.
50. Sillitoe, R.H. Porphyry copper systems. *Econ. Geol.* **2010**, *105*, 3–41. [CrossRef]
51. Ikehata, K.; Maruoka, T. Sulfur isotopic characteristics of volcanic products from September 2014 Mount Ontake eruption, Japan. *Earth Planets Space* **2016**, *68*, 116. [CrossRef]
52. Browne, P.R.L.; Lawless, J.V. Characteristics of hydrothermal eruptions, with examples from New Zealand and elsewhere. *Earth-Sci. Rev.* **2001**, *52*, 299–331. [CrossRef]
53. Gustafson, L.B.; Vidal, C.E.; Pinto, R.; Noble, D.C. Porphyry-epithermal transition, Cajamarca region, Northern Peru. *Soc. Eco. Geo. Spc. Pub.* **2004**, *11*, 279–299.

54. Hedenquist, J.W.; Richard, W.H. Hydrothermal eruptions in the Waiotapu geothermal system, New Zealand: Their origin, associated breccias, and relation to previous metal mineralization. *Econ. Geol.* **1985**, *80*, 1640–1668. [CrossRef]
55. Ohba, T.; Taniguchi, H.; Miyamoto, T.; Hayashi, S.; Hasenaka, T. Mud plumbing system of an isolated phreatic eruption at Akita Yakeyama volcano, northern Honshu, Japan. *J. Volcanol. Geotherm. Res.* **2007**, *161*, 35–46. [CrossRef]
56. John, D.A.; Sisson, T.W.; Breit, G.N.; Rye, R.O.; Vallence, J.W. Characteristics, extent and origin of hydrothermal alteration at Mount Rainier Volcano, Cascades Arc, USA: Implications for debris-flow hazards and mineral deposits. *J. Volcanol. Geotherm. Res.* **2007**, *161*, 35–46. [CrossRef]
57. Browne, P.R.L. Hydrothermal alteration in active geothermal fields. *Annu. Rev. Earth. Pl. Sc.* **1978**, *6*, 229–250. [CrossRef]
58. Hayashi, M. Hydrothermal alteration in the Otake geothermal area, Kyushu. *J. Jpn. Geoth. Energy Assoc.* **1973**, *10*, 9–46, (In Japanese with English abstract).
59. Arribas, A., Jr. Characteristics of high sulfidation deposits, and their relation to magmatic fluid. *Mineral. Soc. Can.* **1995**, *23*, 419–454.
60. Hedenquist, J.W.; Arribas, A., Jr.; Reynolds, T.J. Evolution of an intrusion-centered hydrothermal system: Far southeast-Lepanto porphyry and epithermal Cu-Au deposits, Philippines. *Econ. Geol.* **1998**, *93*, 373–404. [CrossRef]
61. Hedenquist, J.W.; Lowenstern, J.B. The role of magmas in the formation of hydrothermal ore deposits. *Nature* **1994**, *370*, 519–527. [CrossRef]